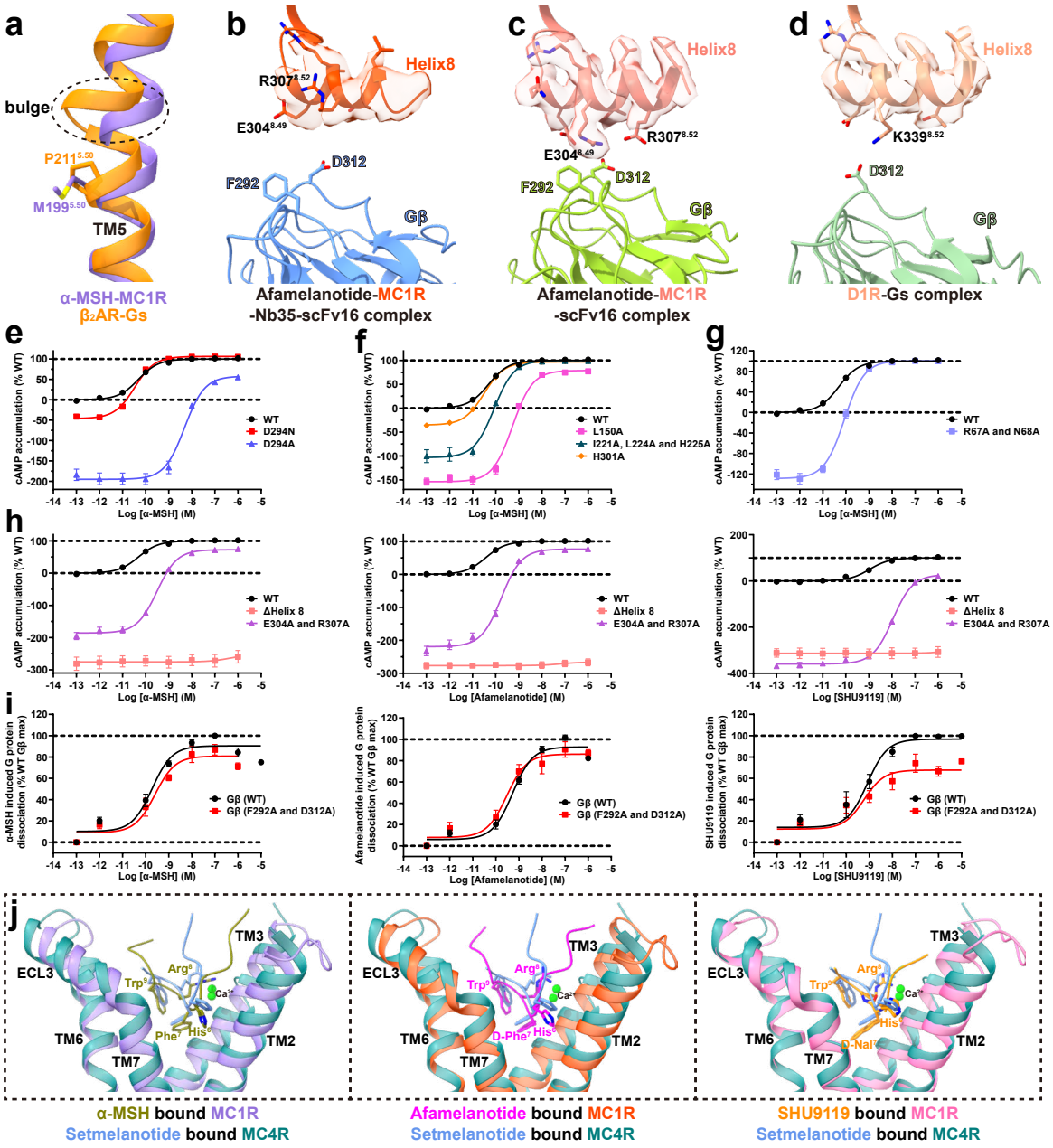

Fig. S6 The mechanism of MC1R activation and Gs coupling. a Structural comparison between $M^{5.50}$ of MC1R (medium purple) and $P^{5.50}$ of β_2AR (PDB: 3SN6, dark orange). The bulge of TM5 is not observed in MC1R. The alignment was based on the structures of MC1R and β_2AR. **b-d** The interactions between helix 8 and Gβ in the afamelanotide-MC1R-Gs-Nb35-scFv16 complex (**b**), afamelanotide-MC1R-Gs-scFv16 complex (**c**) and D1R-Gs complex (**d**, PDB: 7JVP). The EM densities of helix 8 of MC1R and D1R are shown. **e-g** Dose-response curves of cAMP accumulation of the WT and mutated MC1Rs stimulated by α-MSH. Data are presented as means ± S.E.M. of three independent experiments performed in quadruplicate. **h** Dose-response curves of cAMP accumulation of WT MC1R and MC1R with mutations in helix 8 stimulated by α-MSH, afamelanotide and SHU9119. Data are presented as means ± S.E.M. of three independent experiments performed in quadruplicate. **i** α-MSH, afamelanotide and SHU9119 induced G protein activation of WT Gβ and Gβ with mutations in the corresponding residues using NanoBiT assay. Data are presented as means ± S.E.M. of three independent experiments performed in quadruplicate. **j** Structural comparison of the orthosteric binding pockets among α-MSH bound MC1R complex, afamelanotide bound MC1R complex, SHU9119 bound MC1R complex and setmelanotide bound MC4R complex (PDB: 7AUE). The alignment was based on the structures of MC1R and MC4R.